Physico-chemical, photocatalytic and cytotoxicity evaluation of *Annona muricata* L. fruit extract derived zinc oxide nanoparticles in comparison to the commercial chemical version

Ahlam Abdul Aziz[1], V. S. Shaniba[1], P. R. Jayasree[2] and P. R. Manish Kumar[1,*]

Recombinant DNA Laboratory, Department of Biotechnology, and
School of Health Sciences, University of Calicut, Calicut University PO, Malappuram 673 635, India

The present study deployed a sol–gel method, employing an aqueous extract from the fruit of soursop, *Annona muricata* L. for the bio-assisted synthesis of zinc oxide nanoparticles (AmFZnNPs). Following the physico-chemical characterization by UV-Vis spectrometry, Fourier-transform infrared spectroscopy, X-ray diffraction, field-emission scanning electron microscopy and energy-dispersive X-ray spectroscopy, AmFZnNPs were evaluated for photocatalytic and bioactivities in comparison to commercially available chemically-derived zinc oxide nanoparticles (ZnONPs). AmFZnNPs exhibited good photocatalytic and potent antimicrobial activity in comparison to the weak and inefficient action of ZnONPs. Cytotoxicity of AmFZnNPs against colon carcinoma and leukaemic cells conspicuously contrasted with their non-lethality towards human lymphocytes/erythrocytes as well as onion root tip cells whilst ZnONPs displayed high toxicity against all cell types tested except leukaemic cells. Besides the greater acceptability of production via eco-friendly green route, the superiority of AmFZnNPs over their chemically-derived counterparts is clearly demonstrated by our results.

Keywords: *Annona muricata*, antimicrobial, cytotoxicity, nanoparticles, photocatalytic, zinc oxide.

NANOPARTICLES of sizes 100 nm or below display improved or entirely new properties in comparison to their bulkier counterparts in their morphology, size and distribution[1–3]. Physico-chemical methods of synthesizing nanoparticles is expensive and unfit for medical applications due to the use and generation of hazardous chemical agents adsorbed to nanoparticles. An eco-friendly or 'greener' way of nanoparticle synthesis employing plant extracts, thus becomes an attractive alternative system[4]. There are many previous reports on biosynthesis of gold and silver nanoparticles[5–10]. Besides possessing high efficiency of adsorption and catalysis, zinc oxide is a highly attractive metal oxide useful in opto-electro-magnetic and gas-sensing applications[11]. *Aloe barbadensis*, *Aspalathus linearis*, *Poncirus trifoliate* and *Solanum nigrum* are some of the plants, among others, which are being used for the biosynthesis of zinc oxide nanoparticles (ZnONPs)[12–15].

Annona muricata L., commonly called soursop belongs to family Annonaceae. The fruit of this tree is edible and reported with curative properties against cancer, arthritis, malaria, diabetes, inflammation, convulsions, parasitic infections, hypertension, liver ailments and weak immune system[16–19]. The leaves also possess anti-inflammatory, anti-spasmodic, anti-rheumatic, anti-diabetic, anti-cystitis and hepato-protective activities in addition to being an effective antidote against headaches and insomnia[20,21]. Over 400 annonaceous acetogenins from *A. muricata* tree parts have been reported with cytotoxic and anti-tumour activities[22–24].

This paper deals with the biosynthesis of zinc nanoparticles, in the presence of fruit extract of *A. muricata* (AmFZnNPs), deploying a sol–gel technique, enabling controlled production of shape-modulated high purity nanoparticles[25]. Here, we also attempt to bring out a comparison of the physico-chemical aspects and biological activities of AmFZnNPs with those of the chemically-derived, commercially available ZnONPs. AmFZnNPs were characterized employing UV-Vis spectrophotometry, X-ray diffraction (XRD), Fourier-transform infrared spectroscopy (FTIR), energy-dispersive X-ray spectroscopy (EDX) and field-emission scanning electron microscopy (FESEM). Both particle types were evaluated for their potential use as a photocatalyst, antimicrobial and anticancer agent. Photocatalysis was studied using methylene blue dye degradation method whilst the antibacterial activity was ascertained employing clinical bacteria. Comparative cytotoxicities were also determined against human normal lymphocytes/erythrocytes, cancerous colon/leukaemic cell lines, in addition to onion root-tip cells as a plant cell representative. Antiproliferative activities against lymphocytes and onion root-tip cells were analysed using mitotic index (MI) and against cancer cell lines by 3-(4,5-dimethylthiazol-2-yl)-2,5-diphenyltetrazolium bromide (MTT)-based colorimetric

*For correspondence. (e-mail: manishramakrishnan@rediffmail.com)

assay. Percentage haemolysis was accounted for the extent of cellular damage of erythrocytes caused by both types of nanoparticles used.

Materials and methods

Chemicals

Zinc nitrate ($ZnN_2O_6 \cdot 6H_2O$), growth media – DMEM (Dulbecco's Modified Eagle's Medium), RPMI-1640 (Roswell Park Memorial Institute Medium), HiKaryoXL^{TM} RPMI(PHA-P), MTT [3-(4,5-dimethylthiazolyl-2)-2,5-diphenyltetrazolium bromide], acetocarmine stain and antibiotics namely streptomycin and penicillin, were procured from Himedia (Mumbai, India) whereas zinc oxide nanopowder (ZnONPs) (<50 nm) was obtained from Sigma Aldrich (USA). Bacterial media supplements and methylene blue were purchased from SRL, Mumbai. fetal bovine serum (FBS) and Trypsin-EDTA (0.25%) were purchased from Thermo Fisher Scientific (Gibco, USA). All organic solvents used were from Merck Specialities Pvt Ltd (Mumbai). Colon carcinoma HCT116 cells (adherent) and chronic myelogenous leukaemia (suspension) K562 cell lines were obtained from National Centre for Cell Science, Pune, India.

Biosynthesis of AmFZnNPs

Mature fruits of *A. muricata*, collected from Malappuram district (Kerala state) were first washed with tap water followed by a rinse with distilled water. Finely chopped and shade-dried fruit pieces were then ground into a coarse powder. AmFZnNPs were prepared with minor modifications of the procedure reported by Hudlikar *et al.*[26]. A decoction of the fruit powder (10 g) was prepared in 200 ml of deionized, distilled water by boiling for 0.5 h. After cooling, the extract was filtered using autoclaved muslin cloth followed by a further filtration through Whatman No. 1 paper. To varying amounts of this extract (25–75 ml), different concentrations of the metal precursor ranging from 5% to 12% (w/v) was added on reaching 80°C. The solution was allowed to boil for 1 h till it became thicker and assumed a golden yellow colour. It was then subjected to calcinations for a period of 2 h in a ceramic crucible at temperatures ranging from 400°C to 800°C in a muffle furnace. Biosynthesized AmFZnNPs were then ground finely before characterization. For UV-Vis spectrophotometry, photocatalytic, antibacterial and antiproliferative analyses, nanoparticles were sonicated to obtain an aqueous dispersion (5 mg/ml).

Characterization

Optical determination of AmFZnNPs dispersion was determined by UV-Vis spectrophotometry using λ25-Perkin Elmer whilst the purity and crystallinity of particles was assessed with Cu-Kα radiation (40 kV, 15 mA) on a Rigaku miniflex X-ray diffractometer in 2θ ranging from 20° to 80°. Morphological and elemental composition was obtained using Hitachi SEM instrument-S46600 connected to Horiba EDX system. The presence of *A. muricata*-derived capping/stabilizing phyto-constituents adsorbed onto nanoparticle surfaces were analysed by FTIR at wavelengths within 4000–400 cm^{-1} on a Jasco 4100 spectrophotometer. ZnONPs were also subjected to FTIR and FESEM analyses to obtain basic information on their structure and morphology.

Photocatalytic activity

The photocatalytic potential of AmFZnNPs and ZnONPs were assessed by their ability to reduce methylene blue dye into its colourless leuco-form on exposure to direct sunlight[27]. Briefly, AmFZnNPs and ZnONPs each were added separately to 50 ml of methylene blue dye ranging from 200 µg to 2.0 mg/ml and then exposed to direct sunlight for a period of 1, 3 and 5 h respectively. The absorbance at 665 nm was calculated at each time interval using the equation

$$\text{Dye-degradation (\%)} = \frac{(A_0 - A_t)}{A_0} \times 100,$$

where A_0 denotes initial absorption of dye in the presence of test samples and A_t represents absorption of treated dye at time t in hours.

Antibacterial activity

The antimicrobial potentials of AmFZnNPs, aqueous fruit extract (AmF) and that of ZnONPs were tested on clinical isolates, namely *Staphylococcus aureus*, *Pseudomonas aeruginosa*, *Klebsiella pneumoniae* and *Escherichia coli* obtained from a local tertiary care centre. Kirby–Bauer disc diffusion method (CLSI 2017) was used for antibiotic profiling employing commercially available antibiotic discs.

Detemination of MIC and MBC: Exponentially growing bacterial cultures, serially diluted with Luria Bertani (LB) growth medium, were individually exposed to 200–1000 µg/ml of AmFZnNPs, AmF and ZnONPs. Both values of MIC (minimum inhibitory concentration) and MBC (minimum bactericidal concentration) were computed as described earlier employing test cultures and the corresponding untreated controls[28,29].

Agar well diffusion by Kirby–Bauer method: Antibacterial activities of AmFZnNPs, AmF and ZnONPs were confirmed using Kirby–Bauer method[30]. Aliquots (75 µl)

of these three agents were inoculated into 7 mm wells punched out of LB agar plates previously swabbed with each of the four bacterial test strains. The area of bacterial growth inhibition (in mm) was determined after a period of 16 h at 37°C.

Cytotoxicity on HCT116 and K562 cancer cells

MTT assay: The cytotoxicity of AmFZnNPs and ZnONPs on HCT116 and K562 cells were evaluated using MTT assay. In viable cells, mitochondrial succinate dehydrogenase converts the yellow tetrazolium salt into insoluble purple-coloured crystalline formazan, proportional to active cells[31]. HCT116 were cultured in DMEM and the K562 cells were grown in RPMI-1640 media. The growth media contained 10% FBS and antibiotics (100 U/ml penicillin; 100 µg/ml streptomycin). Cell culture maintenance was carried out at 37°C in a humidified CO_2 incubator supplied with 5% CO_2. HCT116 cells were harvested at 85% confluence by trypsinization, whereas the K562 cells were collected at the exponential growth phase. For seeding, 2.5×10^4 of HCT116 and 5×10^4 of K562 cells/ml respectively, were taken and allowed to grow for 24 h. Both cell types were then treated with AmFZnNPs and ZnONPs at concentrations ranging from 25 to 150 µg/ml along with untreated cells serving as controls. The duration of exposure to nanoparticles was 24, 48 and 72 h. The culture medium was then replaced with MTT solution (10 mg/15 ml of phosphate-buffered saline (PBS)). Following a 3 h incubation at 37°C in dark, the reduced formazan crystals were dissolved in dimethyl sulphoxide (DMSO). The optical density (OD) was measured at 570 nm in a plate reader (Thermo Scientific–Multiskan EX)[32,33]. Cellular death (IC_{50} value) was determined as

$$\text{Cell death (\%)} = \frac{(\text{OD}_{\text{control}} - \text{OD}_{\text{treated sample}})}{\text{OD}_{\text{control}}} \times 100.$$

Cytotoxicity on human peripheral blood lymphocytes (hPBLs)

Mitotic Index (MI) analysis: Lymphocytes offer an inexpensive surrogate cell culture system amenable to analysis of MI as a measure of cytotoxicity of various natural and synthetic agents[34]. Self-donated blood (5.0 ml) collected in a heparinized centrifuge tube, was used to check cytotoxicity of nanoparticles on hPBLs. For this, 200 µl of blood was added to 5.0 ml RPMI medium containing PHA (phytohemagglutinin). Following 48 h of growth at 37°C, the hPBLs were exposed to AmFZnNPs and ZnONPs individually at 20, 60 and 100 µg/ml – that is, below, at and above the IC_{50} concentrations – for 24 h; untreated lymphocyte culture served as control. Metaphase arrest was effected by adding colchicine (10 µg/ml) at the 70th h of cell culture. Methanol-acetic acid (3 : 1 v/v) fixation was carried out following hypotonic treatment with pre-warmed 0.075 M KCl and dropped onto clean, frozen and labelled slides. After 30 min of Giemsa staining and air-drying, the slides were observed under microscope using 40 × objective. MI was calculated by scoring 500 cells of both control and treated samples using the formula

$$\text{\% MI} = \frac{\text{Total metaphases}}{\text{Total cells counted}} \times 100,$$

$$\text{\% RMI (relative mitotic index)} = \frac{\text{MI}_{\text{treated}}}{\text{MI}_{\text{control}}} \times 100.$$

Cytotoxicity on erythrocytes

Haemolysis: Release of haemoglobin from damaged erythrocytes can be assessed spectrophotometrically. The buffy coat was removed with a wash of an equal volume of PBS (pH 7.4). This was followed by three washes with PBS by centrifugation step of 5 min at 3000 rpm. An aliquot of the resultant RBC suspension in PBS (0.6 ml) was treated individually with both types of nanoparticles to get a final concentration of 20, 60 and 100 µg/ml for 90 min at 37°C. Distilled water was taken as positive whilst PBS served as negative control. Later, the samples were centrifuged and ODs of the supernatants were measured at 540 nm (refs 35–36). Percentage haemolysis was calculated by

$$\text{\% Haemolysis} = \frac{\text{OD}_{\text{test sample}} - \text{OD}_{\text{PBS}}}{\text{OD}_{\text{distilled water}} - \text{OD}_{\text{PBS}}} \times 100.$$

Morphological examination of treated erythrocytes was carried out using May–Grunwald–Giemsa method[37,38]. In this method, a thin blood smear was prepared on a clean slide, air-dried, fixed in methanol and stained with Giemsa for 30 min and observed under 40× magnification.

Cytotoxicity on onion root-tip cells

Analysis of MI: Onion (*Allium cepa*) root tips, an easily available plant source of dividing apical meristmatic cells, are commonly used to evaluate cellular/genotoxic effects of various physico-chemical and biological agents[39–41]. Healthy bulbs of *A. cepa* collected from local market were soaked in distilled water for root initiation after removing dry scales. On reaching a root length of 1–2 cm, the seedlings were placed individually in distilled water containing 20, 60 and 100 µg/ml of either AmFZnNPs or ZnONPs. Control cells were taken from roots grown in distilled water. The root tips were fixed in Carnoy's mixture following an overnight exposure to nanoparticles solution. Acid-hydrolysis of the root tips

was carried out for 10 min with 1 N HCl and the cells were stained with acetocarmine. Excess dye was removed by a brief destaining step using 45% acetic acid and a further rinse with distilled water[42]. The squash preparation of the root-tip meristem on a clean glass slide was then visualized under 40× objective. MI was scored as percentage of dividing cells in a total of 500 cells.

Analysis of statistical data

The data resulting from triplicate experiments are represented as mean values ± SD (standard deviation). ANOVA (analysis of variance), SPSS version 20.0 was utilized for data analysis by Dunnett's Multiple Comparison test with $P < 0.05$ with respect to control, considered as statistically significant.

Results and discussion

Bio-assisted synthesis of nanoparticles and their characterization

AmFZnNPs were obtained as a pale white nanopowder using 5% (*w*/v) of *A. muricata* AmF containing 10% of $ZnN_2O_6{\cdot}6H_2O$ following calcination at 600°C. The absorption spectrum of AmFZnNPs dispersion was revealed by UV-Vis spectrophotometry. An absorption maxima at 374 nm and 384 nm (Figure 1) clearly revealed the occurrence of intrinsic energy gap absorption of ZnO or its monodispersed particle distribution[43,44]. The absorption of the nanoparticles at the UV region makes them a potential candidate for sunscreen formulations[45].

The FTIR spectra of AmFZnNPs (Figure 2) displayed peaks in the fingerprint region under 1500 cm^{-1}, indicative of ZnONP formation[46]. These zinc nanoparticles (ZnNPs) were observed with their characteristic vibrations peaking sharply at around 400 cm^{-1} (ref. 47). The O–H stretching mode of hydroxyl groups in water, alcohol and phenols at 3432 cm^{-1} observed was apparently attributable to adsorption of water on ZnNPs[48]. The stretching vibrations of C–H and O–H observed at 2922 cm^{-1} and 2853 cm^{-1} respectively, were due to the presence of alkanes and carboxylic acids. The C–N and –C=C– stretch of amide I in proteins and aromatic ring generated corresponding peaks at 1384 cm^{-1}, 1321 cm^{-1} and 1632 cm^{-1} (refs 49–50). Thus, the FTIR spectrum of ZnNPs from *A. muricata* showed the presence of carboxylic acid, amino acids, polyphenols, polysaccharides and proteins. The IR spectrum clearly revealed the occurrence of reduction and stabilization reactions mediated by phyto-biomolecules leading to biosynthesis of ZnNPs.

The diffraction planes (100), (002), (101), (102), (110), (103), (200), (112), (201), (004) and (202) were evident as sharp peaks in the XRD spectra of calcined AmFZnNPs (Figure 3) agreed with JCPDS Card No. 80-0075 which confirmed the occurrence of wurtzite hexagonal structure of ZnONPs[51]. Debye–Scherrer's formula ($D = 0.89\lambda/\beta\cos\theta$)-based computation revealed the size of the particles averaging at 28 nm. The crystalline purity of the biosynthesized AmFZnNPs was reflected in the apparent sharpness of diffraction peaks[52].

Further, FESEM analysis showed individual ZnNPs as well as agglomerates having diameters less than 50 nm (Figure 4). The elemental composition of biosynthesized AmFZnNPs, analysed by EDX (Figure 5) attested to their high purity displaying an elemental composition of only Zn (74.34%) and O (25.66%). The structural identity of chemically-derived ZnONPs used in our study was ascertained by FTIR and FESEM (Figure 6). FTIR spectrum revealed major peaks at 3455 cm^{-1}, 1375 cm^{-1} and

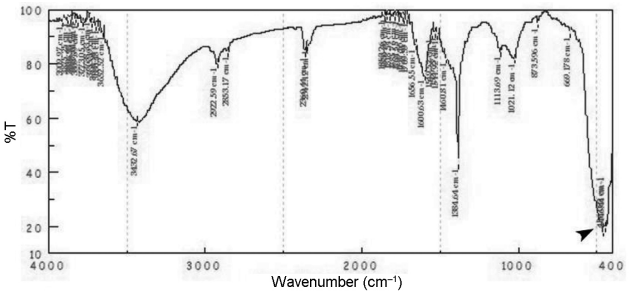

Figure 2. Fourier-transform infrared spectroscopy (FTIR) spectrum of AmFZnNPs.

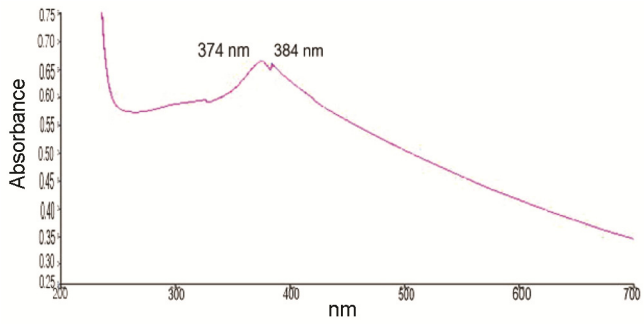

Figure 1. UV-Vis absorption spectrum of AmFZnNPs.

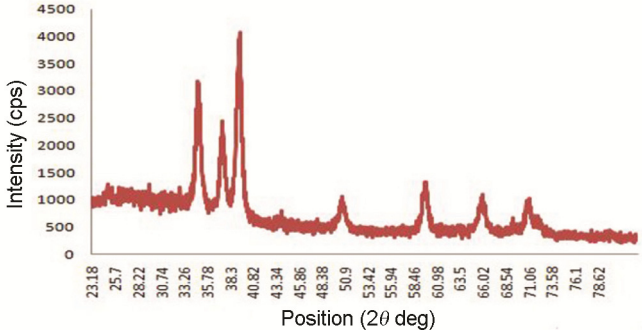

Figure 3. X-ray diffraction pattern of AmFZnNPs.

473 cm^{-1} explaining the vibrations of O–H stretching, C–N of aromatic amines and Zn–O respectively. Unlike the biofabricated AmFZnNPs, ZnONPs were conspicuously denuded of decorations with bioactive compounds. The atomic percentage of oxygen determined by EDX was found to be 58.51 which was relatively higher than the 45.33% value observed for the commercial version of chemically synthesized ZnONPs.

Photocatalytic activity

Methylene blue is a common organic dye discharged from industries into water sources causing water pollution. Previous studies have shown that chemical ZnNPs have photocatalytic dye degradation potential due to surface defects like oxygen vacancies, morphology and size[53]. Likwise, AmFZnNPs were also found to possess good photochemical reactivity and efficiently degraded the toxic dye compared to ZnONPs[54]. At all the concentrations tested, 100% dye degradation was obtained with AmFZnNPs within 5.0 h in a time and dose-dependent manner while ZnONPs showed poor and unpredictable activity. AmFZnNPs have thus proved to be attractive low cost and environmentally sustainable photocatalyst materials (Figure 7).

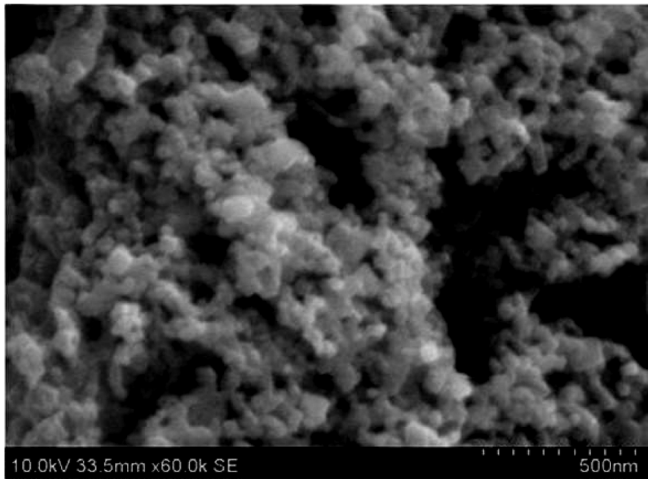

Figure 4. Field-emission scanning electron microscopy (FESEM) micrograph of AmFZnNPs.

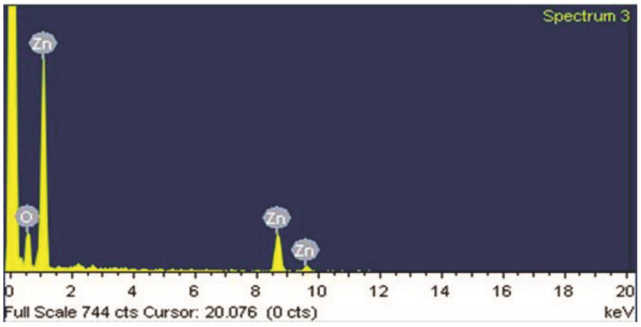

Figure 5. X-ray spectroscopy spectrum of AmFZnNPs.

Antibacterial activity

Antibiotic profiling by Kirby–Bauer method (CLSI, 2017) revealed that *K. pneumoniae* and *S. aureus* were multi-drug resistant. Resistance was observed against antibiotic classes of beta-lactamases, quinolones, aminoglycosides and chloramphenicol. However, *E. coli* was found resistant to only beta-lactamases and quinolones, whilst *P. aeruginosa* displayed resistance against beta-lactamases and lipopeptides. Since the latter two strains showed resistance against only two classes of antibiotics, they do not strictly fulfill the criteria to be 'multi-drug' resistant which requires display of resistance against three or more classes of antibiotics.

The MIC concentrations of AmFZnNPs against the four bacterial strains *S. aureus*, *E. coli*, *K. pneumoniae* and *P. aeruginosa* were determined respectively as 200, 275, 300 and 400 µg/ml whereas the corresponding MBC values were 220, 285, 315 and 410 µg/ml respectively (Table 1). ZnONPs, however, showed antimicrobial activity only against *P. aeruginosa* with a relatively higher MIC at 800 versus 822 µg/ml as the MBC value. This is in line with earlier reports showing biogenic nanoparticles to possess relatively higher antibacterial activity in comparison to chemically-derived ZnNPs[55,56]. Notably, at all concentrations tested in this study, aqueous fruit extract (AmF) *per se* was found to be devoid of any activity against the tested bacterial strains.

The Kirby–Bauer well-diffusion method corroborated well with the MIC values determined (Figure 8, Table 2). The presence of a zone of inhibition of bacterial growth was clearly evident in all four strains treated with AmFZnNPs compared to the single growth inhibition zone obtained with ZnONPs treatment in the case of *P. aeruginosa*. Here again, *A. muricata* extract alone failed to elicit any growth inhibition of the test organisms.

Generation of reactive oxygen species (ROS) on cell surface by ZnONPs is known to enhance membrane permeability and nanoparticle uptake, thereby causing severe bacterial cell wall damage. Also, the amount of oxygen on the surface of nanoparticles has also been found to be directly proportional to the antibacterial activity[57–59]. This is in line with the observed enhanced microbial toxicity of our biogenic nanoparticles. The solubility of free Zn^{2+} ions in culture medium as well as their abrasive cell-surface interactions reportedly contribute towards antimicrobial activity[60,61]. According to Siddiqi *et al.*[62], damage of the cell wall followed by subsequent penetration and accumulation within the cell membrane leads to disruption of its integrity and reduction of surface hydrophobicity. These changes are also accompanied by downregulation of oxidative

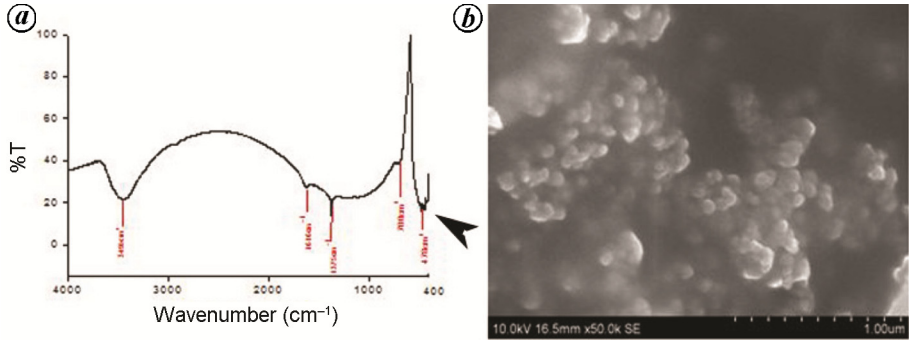

Figure 6. Characterization of chemically-derived ZnONPs. (***a***) FTIR spectrum of ZnONPs and (***b***) FESEM micrograph of ZnONPs.

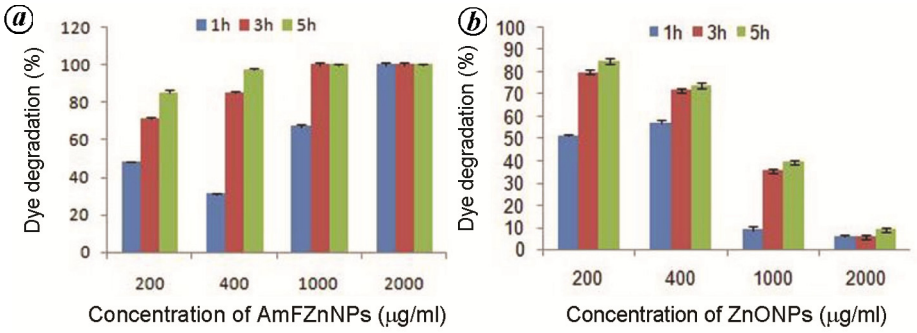

Figure 7. Photocatalytic methylene blue dye-degradation by (***a***) AmFZnNPs and (***b***) ZnONPs.

Table 1. MIC and MBC values of AmFZnNPs and ZnONPs

	Escherichia coli	*Klebsiella pneumoniae*	*Pseudomonas aeruginosa*	*Staphylococcus aureus*
MIC (μg/ml)*				
AmFZnNPs	275 ± 0.56	300 ± 0.48	400 ± 1.3	200 ± 0.78
ZnONPs	–	–	800 ± 1.1	–
MBC (μg/ml)*	*E. coli*	*K. pneumoniae*	*P. aeruginosa*	*S. aureus*
AmFZnNPs	285 ± 1.1	315 ± 0.32	410 ± 0.55	220 ± 1.5
ZnONPs	–	–	822 ± 0.81	–

Values are expressed as mean ± SD, **P* < 0.05 compared to respective controls.

Table 2. Zone of inhibition (in mm) of bacterial growth treated with AmFZnNPs and ZnONPs

Sample*	*E. coli*	*K. pneumoniae*	*P. aeruginosa*	*S. aureus*
AmFZnNPs	20 mm ± 0.03	15 mm ± 0.5	22 mm ± 0.43	20 mm ± 0.12
ZnONPs	–	–	15 mm ± 0.6	–

Values are expressed as mean ± SD, **P* < 0.05 compared to respective controls.

stress-resistance gene transcription and enhancement of ROS (including H_2O_2) – mediated intracellular bacterial killing[62]. Hence, these nanoparticles can be effectively utilized in antibacterial formulations as well as coatings on various biomedical devices to prevent microbial colonization.

Cytotoxicity on HCT116 and K562 cell lines

Cytotoxicity of both types of nanoparticles were individually evaluated by MTT assay, employing HCT116 and K562 cells (Table 3). HCT116 cells exposed to AmFZnNPs showed a time and dose-dependent decrease in the IC_{50} concentrations from 110 μg/ml at 24 h to 68.5 μg/ml at 48 h amounting to a reduction of ~62% in value with an additional reduction of ~12% following a subsequent 24 h treatment period. However, on exposure to ZnONPs, the IC_{50} value was observed to drop by ~57% at 48 h with no further change on continued treatment up to 72 h (Figure 9). On the other hand, in case of K562 cells, the cytotoxicity of bio-derived nanoparticles was observed to reduce by ~43% at 48 h to ~8% at 72 h. On the contrary, the IC_{50}

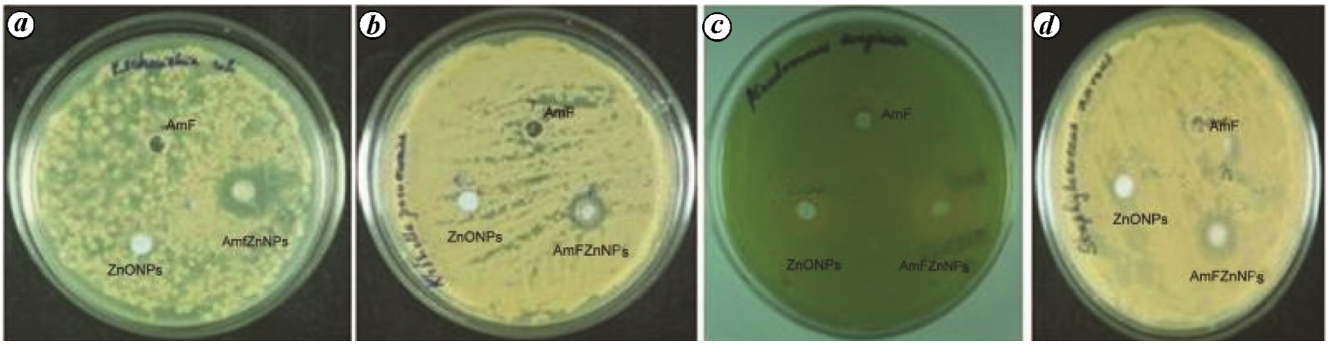

Figure 8. Antibacterial activity, determined by Kirby–Bauer well-diffusion method, against: ***a***, *Escherichia coli*; ***b***, *K. Pneumoniae*; ***c***, *Pseudomonas aeruginosa*; ***d***, *Staphylococcus aureus*.

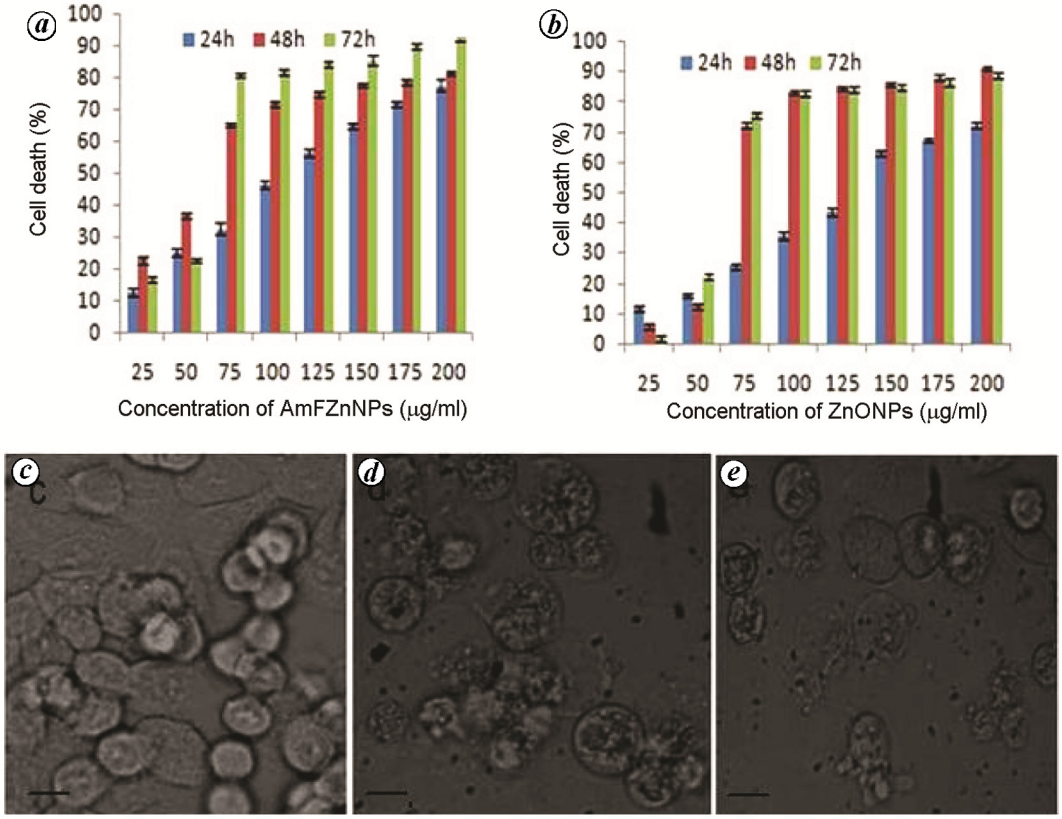

Figure 9. Cytotoxicity against HCT116 cell lines using MTT assay at 24, 48 and 72 h of (***a***) AmFZnNPs and (***b***) ZnONPs and cellular morphology of treated cells by light microscopy (40×), (***c***) control, (***d***) AmFZnNPs (60 μg/ml) and (***e***) ZnONPs (60 μg/ml) treated HCT116 cells. Scale bar – 23 μm.

values in case of ZnONPs against K562 cells were observed to be highest (>150 μg/ml), and strikingly bereft of time and dose-dependent effects (Figure 10). It may be relevant to note that the anticancer effects of nanoparticles become apparent only at about 48 h of treatment which perhaps may be linked to the time period required to attain equilibrium within the cytoplasm after their entry[63]. Overall, a comparison of IC_{50} values clearly indicated a differential, cell-type specific effect produced by both types of ZnONPs. More importantly, these results demonstrated the superiority of biogenic nanoparticles over their chemical counterparts by way of their enhanced cell-killing activity. This may be a consequence of the adsorbed plant-based bioactive compounds on the biogenic nanoparticles, besides variabilities in their penetrance and surface interactions in the light of published reports[64–70].

A dispersion of ZnONPs in aqueous/physiological conditions approximating pH 7.0, have been reported to exhibit positive charge[71]. The pH of aqueous dispersion of commercial ZnONPs used in our study was determined to be about 7.0–7.2. However, in case of biogenic AmFZnNPs, pH in the aqueous phase was determined to be slightly acidic around 6.5, which could be attributable

Table 3. IC_{50} values against HCT116 and K562 cells

	HCT116 (μg/ml)*			K562 (μg/ml)*		
	24 h	48 h	72 h	24 h	48 h	72 h
AmFZnNPs	110 ± 1.4	68.5 ± 0.90 (↓ ~62%)	60 ± 0.78 (↓ ~12%)	124 ± 0.85	70 ± 1.2 (↓ ~43%)	64 ± 0.98 (↓ ~8%)
ZnONPs	140 ± 1.5	60 ± 0.56 (↓ ~57%)	60 ± 1.6 (~57%)	>150	>150	143.8 ± 0.42

Values are expressed as mean ± SD, $*P < 0.05$ compared with the control. ↓ indicates reduction in IC_{50} values.

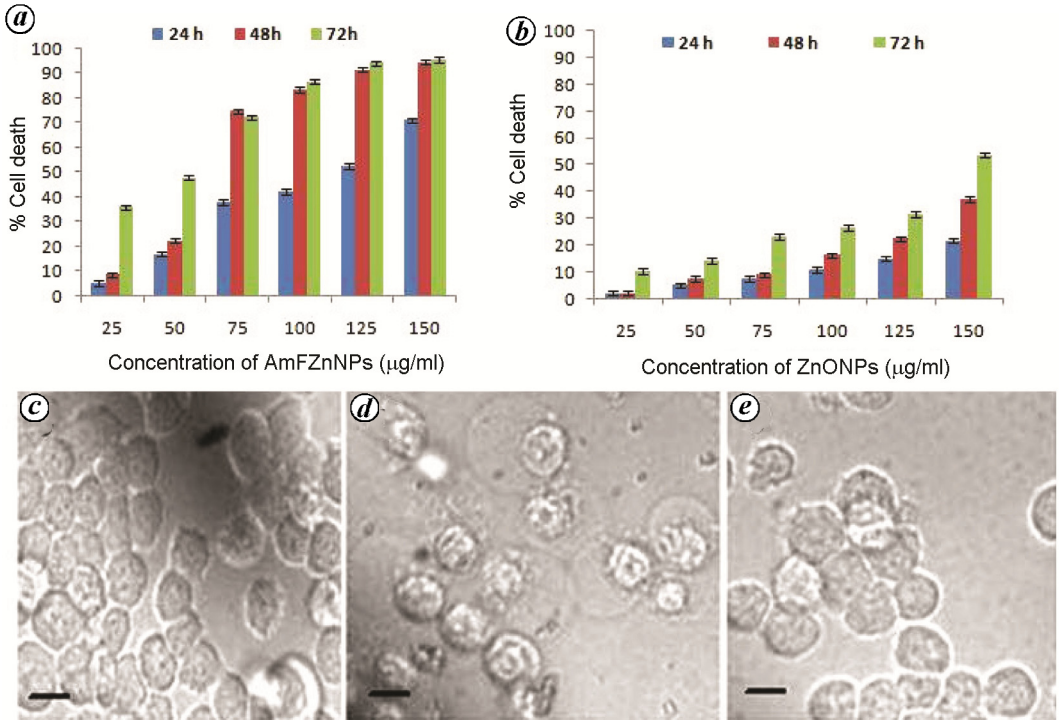

Figure 10. Cytotoxicity against K562 cell lines using MTT assay at 24, 48 and 72 h of (***a***) AmFZnNPs, (***b***) ZnONPs and cellular morphology of treated cells by light microscopy (40×), (***c***) control, (***d***) AmFZnNPs (60 μg/ml) and (***e***) ZnONPs (60 μg/ml) treated K562 cells. Scale bar – 17 μm.

to the aforementioned capped/adsorbed phyto-constituents such as carboxylic acids, polyphenols, polysaccharides, amino acids and proteins as revealed by the FTIR spectrum.

The anticancer activity of ZnONPs were also studied. Notably, cancer cells which usually carry high concentrations of anionic phospholipids and signalling molecules on their surface, attract nanoparticles electrostatically, compared to normal cells. The particles are known to enter the cells directly through the lipid bilayer or by endocytosis into endosomes which merge with lysosomes leading to endosome destabilization. Release of soluble Zn ions triggered due a decrease in pH from 6.3 in the early endosomes, to 5.5 in the late endosomes, further decreasing to 4.7 in the lysosomal compartments, culminates in ROS-mediated apoptosis[71]. Moreover, angiogenesis, a hallmark of cancer cells, leads to irregular and leaky walls with larger gaps than healthy blood vessels giving easy access to nanoparticle entry[72]. Arguably, this also provides a rationale for the selective killing of cancer cells as observed by us.

Cytotoxicity on human peripheral blood lymphocytes

As an indirect measure of the cytotoxicity of AmFZnNPs and ZnONPs on normal human cells, chromosome spreads were examined to determine MI and RMI of treated and controlled lymphocytes. A reduction of 50% and above in RMI values is considered to be indicative of cytotoxicity[73]. The results showed that the decrease in

Table 4. MI and RMI of AmFZnNPs and ZnONPs treated hPBLs

	AmFZnNPs		ZnONPs	
Concentration (μg/ml)	MI (%)*	RMI (%)	MI (%)*	RMI (%)
20	6.95 ± 0.32	93.8	4.8 ± 0.78	64.8
60	6.40 ± 0.58	86.4	2.1 ± 0.55	28.3
100	5.80 ± 0.21	78.3	0.5 ± 0.32	6.7

MI of untreated control cells (7.41 ± 0.93) was taken as 100% to compute the RMI values. Values are expressed as mean ± SD, $*P < 0.05$ compared to controls.

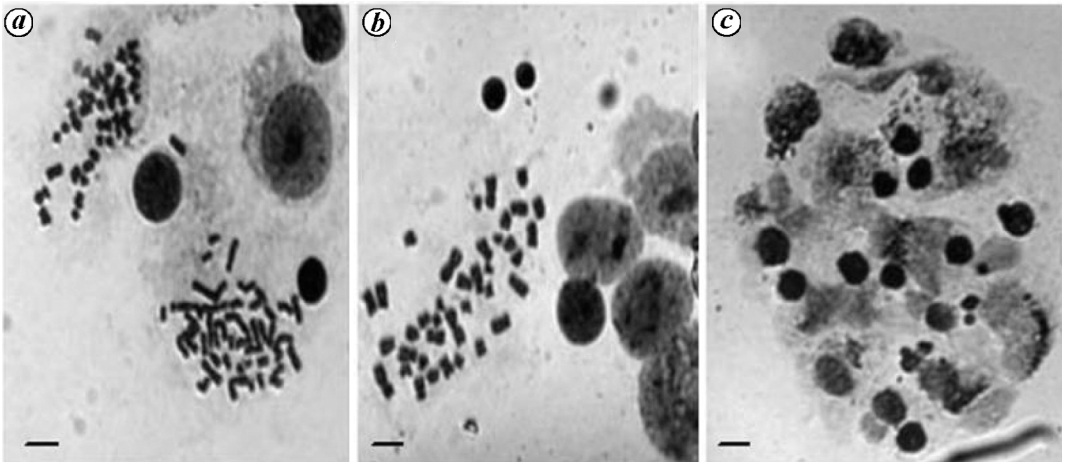

Figure 11. Cytotoxicity of AmFZnNPs and ZnONPs against hPBLs studied by preparation of Giemsa stained metaphase spread (40×). (***a***) Control, (***b***) AmFZnNPs (60 μg/ml) and (***c***) ZnONPs (60 μg/ml). Scale bar – 15 μm.

RMI of AmFZnNPs treated cells ranged from ~7% to 23% as against a drastic ~46% to 95% reduction observed due to exposure to the ZnONPs (Table 4). In other words, the biogenic nanoparticles were well within the biosafety limits even at the highest concentration tested (100 μg/ml) compared to their chemically-derived counterparts which were toxic beyond 20 μg/ml. Light microscopy of ZnONPs treated cells clearly revealed extensive damage to cellular morphology as evidenced by the loss of well-defined cell shape, apparently due to membrane disruption with near complete absence of metaphase chromosomes (Figure 11). These observations are in line with earlier studies on ZnONP-induced cellular and genotoxic effects such as decrease in MI accompanied with chromosomal aberrations including chromosomal breaks in hPBLs[74,75]. Lipid peroxidations leading to alterations in cell membrane, oxidative DNA damage and induction of mitochondria-mediated apoptosis have also been reported[76–78].

Haemolysis of erythrocytes

Given the fact that 5% haemolysis is permissible for biomaterials, significant haemolytic activity was not observed in cells treated with either of the two types of nanoparticles tested[79]. However, ZnONPs treatment resulted in a marginal increase of haemolytic index up to 7% at the highest dose tested. Noticeably, erythrocytes exposed to ZnONPs when stained with Giemsa, were observed to be relatively shrunken size-wise displaying sharp angular membrane distortions but with minimal haemolysis (Figure 12), similar to those described by Shirsekar *et al.*[80]. Incidentally, similar structurally distorted erythrocytes with lost concavity, typical of echinocytes have been reportedly induced on exposure to certain aqueous plant extracts[81]. This may be attributed to the inherent nature of these agents to modify erythrocyte membrane-related ionic/osmotic transport balance[82]. However, such morphological distortions were virtually absent in AmFZnNPs-treated red blood cells. A recent report by Babu *et al.*[83] provided supportive evidence, wherein the presence of natural agent ferulic acid was found to reduce the haemolytic activity of ZnONPs resulting in better biocompatibility[83]. It is quite tempting to speculate that the biogenic AmFZnNPs generated by us carrying infinitesimally small amounts of adsorbed phytoconstituents of *A. muricata* do not apparently affect the erythrocytes as evidenced by their normal cytomorphology.

Cytotoxicity on A. cepa root-tips

A dose-dependent reduction in MI of about 30% was observed in AmFZnNPs-treated onion root meristematic

Table 5. MI of AmFZnNPs and ZnONPs treated *Allium cepa* root-tip cells

	AmFZnNPs		ZnONPs	
Concentration (μg/ml)	MI (%)*	RMI (%)	MI (%)*	RMI (%)
20	12.82 ± 0.46	90.9	0.9 ± 1.2	6.4
60	11.6 ± 0.69	82.2	–	
100	9.9 ± 0.4	70.2	–	

MI of untreated control cells (14.1 ± 1.03) was taken as 100% to compute the RMI values. Values are expressed as mean ± SD, $*P < 0.05$ compared to controls.

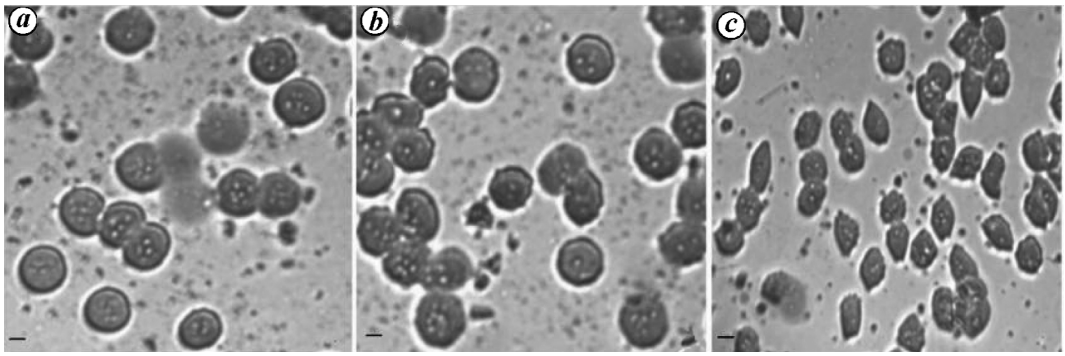

Figure 12. Morphologic evaluation of AmFZnNPs and ZnONPs treated erythrocytes stained with Giemsa (40×). ***a***, Control; ***b***, AmFZnNPS (60 μg/ml); ***c***, ZnONPs (60 μg/ml). Scale bar – 7 μm.

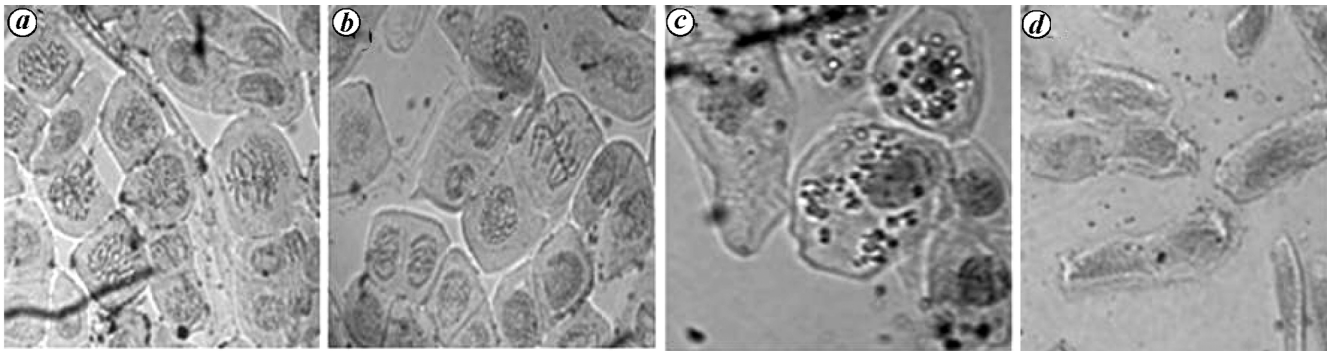

Figure 13. Cytotoxicity of AmFZnNPs and ZnONPs against *A. cepa*. ***a***, Control; ***b***, AmFZnNPs (60 μg/ml); ***c***, ZnONPs (20 μg/ml); ***d***, ZnONPs (60 μg/ml).

cells at the highest concentration tested (Table 5). However, ZnONPs treatment induced drastic cytogenotoxicity on these plant cells characterized by a near complete absence of mitotic phases and formation of ghost cells (Figure 13). Previous reports on the cytogenetic toxicity of ZnONPs on onion root-tip cells mention the observation of extensive cell vacuolation along with ruptured nuclear and plasma membranes[84,85]. Again, cells exposed to biogenic nanoparticles, however, failed to display such cytological defects.

Conclusion

Employing the aqueous extract of *Annona muricata* fruit, biogenic zinc oxide nanoparticles were successfully synthesized by an eco-friendly, simple and rapid, sol–gel technique. Their enhanced photocatalytic, antimicrobial and anticancer activities in comparison to their chemically-synthesized counterparts make them versatile for exploitation in biomedical and technological applications. The present study also provided proof of principle with regard to toxicity of biosynthesized nanoparticles which selectively targeted human colon and leukaemic cancer cells whilst being biocompatible and apparently innocuous to the tested normal human (lymphocytes/erythrocytes) and plant cell models.

Conflict of interest: No conflict of interest has been declared by any of the authors.

1. Sabir, S., Arshad, M. and Chaudhari, S. K., Zinc oxide nanoparticles for revolutionizing agriculture: synthesis and applications. *Sci. World J.*, 2014, **2014**, 1–8.

2. Govindasamy, R. *et al.*, Novel and simple approach using synthesized nickel nanoparticles to control blood-sucking parasites. *Vet. Parasitol.*, 2013, **191**, 332–339.
3. Singh, P. R., Shukla, V. K., Yadav, R. S., Sharma P. K., Singh, P. K. and Pandey, A. C., Biological approach of zinc oxide nanoparticles formation and its characterization. *Adv. Mat. Lett.*, 2011, **2**, 313–317.
4. Nagarajan, S. and Kuppusamy, K. A., Extracellular synthesis of zinc oxide nanoparticle using seaweeds of gulf of Mannar, India. *J. Nanobiotechnol.*, 2013, **34**, 209–214.
5. Elia, P., Zach, R., Hazan, S., Kolusheva, S., Porat, Z. and Zeiri, Y., Green synthesis of gold nanoparticles using plant extracts as reducing agents. *Int. J. Nanomed.*, 2014, **9**, 4007–4021.
6. Kumar, B., Smita, K., Cumbal, L. and Debut, A., Synthesis of silver nanoparticles using Sacha inchi (*Plukenetia volubilis* L.) leaf extracts. *Saudi J. Biol. Sci.*, 2014, **21**, 605–609.
7. Kotakadi, V. S., Rao, Y. S., Gaddam, S. A., Prasad, T. N., Reddy, A. V. and Gopal, D. V., Simple and rapid biosynthesis of stable silver nanoparticles using dried leaves of *Catharanthus roseus* and its anti microbial activity. *Colloid. Surf. B*, 2013, **105**, 194–198.
8. Krishnamurthy, N. B., Nagaraj, B., Malakar, B., Liny, P. and Dinesh, R., Green synthesis of gold nanoparticles using *Tagetes erecta* L (Marigold) flower extract and evaluation of their antimicrobial activities. *Int. J. Pharm. Biol. Sci.*, 2012, **3**, 212–221.
9. Ponarulselvam, S., Panneerselvam, C., Murugan, K., Aarthi, N., Kalimuthu, K. and Thangamani, S., Synthesis of silver nanoparticles using leaves of *Catharanthus roseus* Linn. G. Don and their antiplasmodial activities. *Asian Pac. J. Trop. Biomed.*, 2012, **2**, 574–580.
10. Padma, S. V. and Dhara, S., Biosynthesis of silver nanoparticles using lemon leaves extract and its application for antimicrobial finish on fabric. *Appl. Nanosci.*, 2012, **2**, 163–168.
11. Rizwan, W., Amrita, M., Soon, Y., Young-Soon, K. and Hyung-Shik, S., Antibacterial activity of ZnO nanoparticles prepared via non- hydrolytic solution route. *Appl. Microbiol. Biotechnol.*, 2010, **87**, 1917–1925.
12. Sangeetha, G., Rajeswari, S. and Venckatesh, R., Green synthesis of zinc oxide nanoparticles by *Aloe barbedensis miller* leaf extract: structure and optical properties. *Mater. Res. Bull.*, 2011, **46**, 2560–2566.
13. Diallo, A., Ngom, B. D., Park, E. and Maaza, M., Green synthesis of ZnO nanoparticles by *Aspalathus linearis*: structural and optical properties. *J. Alloy. Compd.*, 2015, **646**, 425–430.
14. Nagajyothi, P. C., Minh, T. N., Sreekanth, T. V. M., Lee, J., Lee, D. J. and Lee, K. D., Green route biosynthesis: characterization and catalytic activity of ZnO nanoparticles. *Mater. Lett.*, 2013, **108**, 160–163.
15. Ramesh, M., Anbuvannan, M. and Viruthagiri, G., Green synthesis of ZnO nanoparticles using *Solanum nigrum* leaf extract and their antibacterial activity. *Spectrochim. Acta A*, 2015, **136**, 864–870.
16. Patel, S. and Patel, J. K., A review on a miracle fruits of *Annona muricata*. *J. Pharmacogn. Phytochem.*, 2016, **5**, 137–148.
17. Ishola, I. O., Awodele, O., Olusayero, A. M. and Ochieng, C. O., Mechanisms of analgesic and anti-inflammatory properties of *Annona muricata* Linn. (Annonaceae) fruit extract in rodents. *J. Med. Food*, 2014, **17**, 1375–1382.
18. Astirin, O., Artanti, A., Fitria, M., Perwitasari, E. and Prayitno, A., *Annona muricata* Linn leaf induce apoptosis in cancer cause virus. *J. Cancer Ther.*, 2013, **4**, 1244–1250.
19. Ferreira, L., Castro, P., Chagas, A., Franca, S. and Beleboni, R., In vitro anthelmintic activity of aqueous leaf extract of *Annona muricata* L. (Annonaceae) against *Haemonchus contortus* from sheep. *Exp. Parasitol.*, 2013, **134**, 327–332.
20. Hamizah, S., Roslida, A. H., Fezah, O., Tan, K. L., Tor, Y. S. and Tan, C. I., Chemopreventive potential of *Annona muricata* L leaves on chemically-induced skin papillomagenesis in mice. *Asian Pac. J. Cancer Prev.*, 2012, **13**, 2533–2539.
21. de Sousa, O. V., Vieira, G. D., de Jesus, R. G., de Pinho, J., Yamamoto, C. H. and Alves, M. S., Antinociceptive and anti-inflammatory activities of the ethanol extract of *Annona muricata* L. leaves in animal models. *Int. J. Mol. Sci.*, 2010, **11**, 2067–2078.
22. Han, B., Wang, T. D., Shen, S. M., Yu, Y., Mao, C., Yao, Z. J. and Wang, L. S., *Annonnaceous acetogenin* mimic AA005 induces cancer cell death via apoptosis inducing factor through a caspase-3-independent mechanisms. *BMC Cancer*, 2015, **15**, 139.
23. Moghadamtousi, S. Z., Fadaeinasab, M., Nikzad, S., Mohan, G., Ali, H. M. and Kadir, H. A., *Annona muricata* (Annonaceae): a review of its traditional uses, isolated acetogenins and biological activities. *Int. J. Mol. Sci.*, 2015, **16**, 15625–15658.
24. Rupprecht, J. K., Hui, Y. H. and McLaughlin, J. L., *Annonaceous acetogenins*: a review. *J. Nat. Prod.*, 1990, **53**, 237–278.
25. Samat, N. A. and Roslan, M. N., Sol–gel synthesis of zinc oxide nanoparticles using *Citrus aurantifolia* extracts. *Ceram. Int.*, 2013, **39**, S545–S548.
26. Hudlikar, M., Shreeram, J., Mayur, D. and Kisan, K., Latex-mediated synthesis of ZnS nanoparticles: green synthesis approach. *J. Nanopart. Res.*, 2012, **14**, 865.
27. Bandekar, G., Rajurkar, N. S., Mulla, I. S., Mulik, U. P., Amalnerkar, D. P. and Adhyapak, P. V., Synthesis, characterization and photocatalytic activity of PVP stabilized ZnO and modified ZnO nanostructures. *Appl. Nanosci.*, 2014, **4**, 199–208.
28. Salem, W., Leitner, D. R. and Zingl, F. G., Antibacterial activity of zinc and silver nanoparticles against *Vibrio cholera* and enterotoxic *Escherichia coli*. *Int. J. Med. Microbiol.*, 2015, **305**, 85–95.
29. Reddy, L. S., Nisha, M. M., Joice, M. and Shilpa, P. N., Antimicrobial activity of zinc oxide (ZnO) nanoparticle against *Klebsiella pneumoniae*. *Pharm. Biol.*, 2014, **52**, 1388–1397.
30. Vani, C., Sergin, G. K. and Annamalai, A., A study on the effect of zinc oxide nanoparticles in *Staphylococcus aureus*. *Int. J. Pharm. Biol. Sci.*, 2011, **2**, 326–335.
31. Sahu, D., Kannan, G. M., Tailang, M. and Vijayaraghavan, R., In vitro cytotoxicity of nanoparticles: a comparison between particle size and cell type. *J. Nanosci.*, 2016, **2016**, 1–9.
32. Sanaeimehr, Z., Javadi, I. and Namvar, F., Antiangiogenic and antiapoptotic effects of green – synthesized zinc oxide nanoparticles using *Sargassum muticum* algae extraction. *Cancer Nanotechnol.*, 2018, **9**, 3.
33. Namvar, F., Rahman, H. S., Mohamad, R., Azizi, S., Tahir, P. M., Chartrand, M. S. and Yeap, S. K., Cytotoxic effects of biosynthesized zinc oxide nanoparticles on murine cell lines. *Evid.-Based Complement. Alternat. Med.*, 2015, **2015**, 1–11.
34. Montoro, A., Soriano, J. M. and Barquinero, J. F., Assessment in vitro of cytogenetic and genotoxic effects of propolis on human lymphocytes. *Food Chem. Toxicol.*, 2012, **50**, 216–221.
35. Khan, M., Naqvi, A. H. and Ahmad, M., Comparative study of the cytotoxic and genotoxic potentials of zinc oxide and titanium dioxide nanoparticles. *Toxicol. Rep.*, 2015, **2**, 765–774.
36. Raguvaran, R., Manuja, A., Singh, S., Chopra, M., Manuja, B. K. and Dimri, U., Zinc oxide nanoparticles induced hemolytic cytotoxicity in horse red blood cells. *Int. J. Pharm. Sci. Res.*, 2015, **6**, 1166–1169.
37. Junqueira, L. C. and Carneiro, J., *Histologia basica*. Guanabara Koogan, Rio de Janeiro, 2004, **8**, 285–300.
38. World Health Organization, Quality control of Giemsa stock solution and buffered water, 2016, 1–11; http://www.wpro.who.int/mvp/lab_quality/2096_oms_gmp_sop_03c_rev.pdf (accessed on 11 February 2018).
39. Obute, G. C., Ekeke, C. and Izuka, D. C., Genotoxicity assessment of refined petroleum products and popular local soft drink (Zobo) in daily use in Nigeria. *Res. J. Mutagen.*, 2016, **6**, 22–30.
40. Taranath, T. C., Bheemanagouda, N. P., Santosh, T. U. and Sharath, B. S., Cytotoxicity of zinc nanoparticles fabricated by *Justicia adathoda* L. on root tips of *Allium cepa* L. – a model approach. *Environ. Sci. Pollut. Res.*, 2015, **22**, 8611–8617.

41. Pandey, H., Kumar, V. and Roy, B. K., Assessment of genotoxicity of some common food preservatives using *Allium cepa* L. as a test plant. *Toxicol. Rep*., 2014, **1**, 300–308.
42. Bhagyanathan, N. K. and Thoppil, J. E., Pre-apoptotic activity of aqueous extracts of *Cynanchum sarcomedium* Mieve & Liede on cells of *Allium cepa and* human erythrocytes. *Protoplasma*, 2016, **253**, 1433–1438.
43. Talam, S., Karumuri, S. R. and Gunnam, N., Synthesis, characterization and spectroscopic properties of ZnO nanoparticles. *ISRN Nanotechnol*., 2012, **2012**, 1–6.
44. Zak, A. K., Razali, R., Abd Majid, W. H. and Darroudi, M., Synthesis and characterization of a narrow size distribution zinc oxide nanoparticles. *Int. J. Nanomed*., 2011, **6**, 1399–1403.
45. Majid, D., Zahra, S., Reza, K. O., Ali, K. Z., Hadi, K. and Mohamad, H. N., Sol–gel synthesis, characterization, and neurotoxicity effect of zinc oxide nanoparticles using gum tragacanth. *Ceram. Int*., 2013, **39**, 9195–9199.
46. John, C., Interpretation of infrared spectra, a practical approach. *Encyclopedia Analytical Chemistry*, John Wiley and Sons, USA, 2000, 10815–10837.
47. Rajendran, S. P. and Sengodan, K., Synthesis and characterization of zinc oxide and iron oxide nanoparticles using *Sesbania grandiflora* leaf extract as reducing agent. *J. Nanosci*., 2017.
48. Senthilkumar, S. R. and Sivakumar, T., Green tea (*Camellia sinensis*) mediated synthesis of zinc oxide (ZnO) nanoparticles and studies on their antimicrobial activities. *Int. J. Pharm. Pharm. Sci*., 2014, **6**, 461–465.
49. Dobrucka, R. and Dugaszewska, J., Biosynthesis and antibacterial activity of ZnO nanoparticles using *Trifolium pretense* flower extract. *Saudi J. Biol. Sci*., 2016, **23**, 517–523.
50. Chandrasekhar, N. and Vinay, S. P., Yellow colored blooms of *Argemone Mexicana* and *Turnera ulmifolia* mediated synthesis of silver nanoparticles and study of their antibacterial and antioxidant activity. *Appl. Nanosci*., 2017, **7**, 851–861.
51. Gnanasangeetha, D. and Sarala, T. D., Biogenic production of zinc oxide nanoparticles using *Acalypha Indica*. *J. Chem. Biol. Phys. Sci*., 2014, **4**, 238–246.
52. Bhuyan, T., Kavita, K., Khanuja, M., Prasad, R. and Varma, A., Biosynthesis of zinc oxide nanoparticles from *Azadirachta indica* for antibacterial and photocatalytic applications. *Mat. Sci. Semicon. Proc*., 2015, **32**, 55–61.
53. Davar, F., Majedi, A. and Mirzaei, A., Green synthesis of ZnO nanoparticles and its application in the degradation of some dyes. *J. Am. Ceram. Soc*., 2015, **98**, 1739–1746.
54. Suresh, D., Nethravathi, P. C., Udayabhanu, Rajanaika, H., Nagabhushana, H. and Sharma, S. C., Green synthesis of multifunctional zinc oxide (ZnO) nanoparticles using *Cassia fistula* plant extract and their photodegradative, antioxidant and antibacterial activities. *Mat. Sci. Semicon.. Proc*., 2015, **3**, 1446–1454.
55. Gunalan, S., Sivaraj, R. and Rajendran, V., Green synthesized ZnO nanoparticles against bacterial and fungal pathogens. *Prog. Nat. Sci: Mater. Int*., 2012, **2**, 693–700.
56. Emami-Karvani, Z. and Chehrazi, P., Antibacterial activity of ZnO nanoparticle on Gram-positive and Gram-negative bacteria. *Afr. J. Microbiol. Res*., 2011, **5**, 1368–1373.
57. Ali, K., Dwivedi, S., Azam, A., Saquib, Q., Al-Said, M. S., Al khedhairy, A. A. and Musarrat, J., *Aloe vera* extract functionalized zinc oxide nanoparticles as nanoantibiotics against multi-drug resistant clinical bacterial isolates. *J. Colloid Interf. Sci*., 2016, **472**, 145–156.
58. Sirelkhatim, A. *et al.*, Review on zinc oxide nanoparticles: antibacterial activity and toxicity mechanism. *Nano-Micro Lett*., 2015, **7**, 219–242.
59. Xie, Y., He, Y., Irwin, P. L., Jin, T. and Shi, X., Antibacterial activity and mechanism of action of zinc oxide nanoparticles against *Campylobacter jejuni*. *Appl. Environ. Microbiol*., 2011, **77**, 2325–2331.
60. Raghupathi, K. R., Koodali, R. T., Manna, A. C., Size-dependent bacterial growth inhibition and mechanism of antibacterial activity of zinc oxide nanoparticles. *Langmuir*, 2011, **27**, 4020–4028.
61. Pati, R. *et al.*, Topical application of zinc oxide nanoparticles reduces bacterial skin infection in mice and exhibits antibacterial activity by inducing oxidative stress response and cell membrane disintegration in macrophages. *Nanomed.: Nanotechnol., Biol. Med.*, 2014, **10**, 1195–1208.
62. Siddiqi, K. S., Rahman, A., Tajuddin and Husen, A., Properties of zinc oxide nanoparticles and their activity against microbes. *Nanoscale Res. Lett.*, 2018, **13**, 141(1–13).
63. Alarifi, S., Ali, D., Alkahtani, S., Verma, A., Ahamed, M., Ahmed, M. and Alhadlaq, H. A., Induction of oxidative stress, DNA damage and apoptosis in a malignant human skin melanoma cell line after exposure to zinc oxide nanoparticles. *Int. J. Nanomed.*, 2013, **8**, 983–993.
64. Moghaddam, A. B., Moniri, M., Azizi, S., Rahim, R. A., Ariff, A. B., Navaderi, M. and Mohamad, R., Eco-friendly formulated zinc oxide nanoparticles: induction of cell cycle arrest and apoptosis in the MCF-7 cancer cell line. *Genes*, 2017, **8**, 281.
65. Biplab, K. C., Paudel, S. N., Rayamajhi, S., Karna, D., Adhikari, S., Shrestha, B. G. and Bisht, G. K. C., Enhanced preferential cytotoxicity through surface modification: synthesis, characterization and comparative *in vitro* evaluation of TritonX-100 modified and unmodified zinc oxide nanoparticles in human breast cancer cell (MDA-MB-231). *Chem. Cent. J.*, 2016, **10**, 16.
66. Venkatesan, J., Kim, S. K. and Shim, M. S., Antimicrobial, antioxidant and anticancer activities of biosynthesized silver nanoparticles using algae *Ecklonia cava*. *Nanomaterials*, 2016, **6**, 235.
67. Geetha, R., Ashokkumar, T., Tamilselvan, S., Govindaraju, K., Sadiq, M. and Singaravelu, G., Green synthesis of gold nanoparticles and their anticancer activity. *Cancer Nanotechnol.*, 2013, **4**, 91–98.
68. Premanathan, M., Karthikeyan, K., Jeyasubramanian, K. and Manivannan, G., Selective toxicity of ZnO nanoparticles towards gram positive bacteria and cancer cells by apoptosis through lipid peroxidation. *Nanomedicine*, 2011, **7**, 184–192.
69. Rasmussen, J. W., Martinez, E., Louka, P. and Wingett, D. G., Zinc oxide nanoparticles for selective destruction of tumor cells and potential for drug delivery applications. *Expert Opin. Drug Deliv*., 2010, **7**, 1063–1077.
70. Tso, C., Zhung, C., Shih, Y., Tseng, Y., Wu, S. and Doong, R., Stability of metal oxide nanoparticles in aqueous solutions. *Water Sci. Technol*., 2010, **61**(1), 127–133.
71. Bisht, G. and Rayamajhi, S., ZnO nanoparticles: a promising anticancer agent. *Nanobiomedicine*, 2016, **3**(9), 1–11.
72. Grossman, H. J. and McNeil, S. E., Nanotechnology in cancer medicine. *ACS Nano*, 2012, **4**(10), 5641–5646.
73. Health Effects Test Guidelines, United States Environmental Protection Agency. Prevention, Pesticides and Toxic Substances (7101), EPA 712-C-98-223, 1998.
74. Gümüş, D., Berber, A. A., Ada, K. and Aksoy, H., *In vitro* genotoxic effects of ZnO nanomaterials in human peripheral lymphocytes. *Cytotechnology*, 2014, **66**, 317–325.
75. Mussarat, J., Saquib, Q., Azam, A. and Naqvi, S. A. H., Zinc oxide nanoparticles induced-DNA damage in human lymphocytes. *Int. J. Nanopart.*, 2009, **2**, 402–414.
76. Horie, M. and Fujita, K., Chapter four-toxicity of metal oxides nanoparticles. *Adv. Mol. Toxicol*., 2011, **5**, 145–178.
77. Lin, W., Xu, Y., Huang, C., Ma, Y., Shannon, K. B., Chen, D. and Huang, Y., Toxicity of nano- and micro-sized zinc oxide particles in human lung epithelial cells. *J. Nanopart. Res*., 2009, **11**, 25–39.
78. Rikans, L. E. and Hornbrook, K. R., Lipid peroxidation, antioxidant protection and aging. *Biochem. Biophys. Acta*, 1997, **1362**, 116–127.

79. Das, D., Nath, B. C., Phukon, P., Kalita, A. and Dolui, S. K., Synthesis of ZnO nanoparticles and evaluation of antioxidant and cytotoxic activity. *Colloid Surf. B*, 2013, **111**, 556–560.
80. Shirsekar, P. P., Kanhe, N. S. and Mathe, V. L., Interaction of zinc oxide nanoparticles with human red blood cells. *Bionano Front.*, 2016, **9**, 99–104.
81. Maiworm, A. I., Presta, G. A., Santos-Filho, S. D., Paoli, S. D., Giani, T. S., Fonseca, A. S. and Bernardo-Filho, M., Osmotic and morphological effects on red blood cell membrane: action of an aqueous extract of *Lantana camara*. *Braz. J. Pharmacogr.*, 2008, **18**, 42–46.
82. Prajitha, V. and Thoppil, J. E., Cytotoxic and apoptotic activities of extract of *Amaranthus spinosus* L. in *Allium cepa* and human erythrocytes. *Cytotechnology*, 2017, **69**, 123–133.
83. Babu, E. P. *et al.*, Size dependent uptake and hemolytic effect of zinc oxide nanoparticles on erythrocytes and biomedical potential of ZnO-Ferulic acid conjugates. *Sci. Rep.*, 2017, **7**, 4203(1–12).
84. Ghosh, M. *et al.*, Effect of ZnO nanoparticles in plants: cytotoxicity, genotoxicity, deregulation of antioxidant defenses and cell cycle arrest. *Mutat. Res.-Genet. Toxicol. Environ. Mutagen*, 2016, **807**, 25–32.
85. Kumari, M., Khan, S. S., Pakrashi, S., Mukherjee, A. and Chandrasekaran, N., Cytogenetic and genotoxic effects of zinc oxide nanoparticles on root cells of *Allium cepa*. *J. Hazard. Mater.*, 2011, **190**, 613–621.

ACKNOWLEDGEMENTS. We thank the National Institute of Technology, Calicut, for providing FESEM-EDX facility. We also thank Physics and Chemistry Department of Calicut University for technical assistance with XRD and FTIR analyses. A. A. A. acknowledges receipt of INSPIRE fellowship (IF140004) awarded by DST, Govt of India.

Received 16 November 2018; revised accepted 11 April 2019

doi: 10.18520/cs/v117/i9/1492-1504